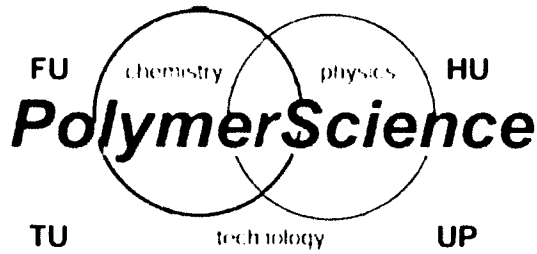

Master of Science Program in Polymer Science

of the Freie Universität Berlin, Humboldt-Universität zu Berlin, Technische Universität Berlin, and Universität Potsdam

Polymerization of Carbon Nitride

-experimental and theoretical investigation

BY

Jie Cao

March 22nd, 2006

Germany

I, **Jie Cao**, formally submit my thesis

Polymerization to Carbon Nitride -experimental and theoretical investigation

in fulfillment of the requirements set forth by the Master of Science of Polymer Science program.

I hereby certify that the work presented in this thesis is my own original work and has been based on the research I performed during the second year of the Master of Science Program and by using only the means and source material as noted therein.

Jie Cao

SUPERVISORS

Professor Markus Antonietti
Director of Colloid Department, Max-Planck-Institute
Professor Matthias Scheffler
Director of Theory Department, Fritz-Haber-Institute of Max-Planck-Institute
Dr. Arne Thomas
Group Leader of Colloid Department, Max-Planck-Institute
Dr. Johan Carlsson
Group Leader of Theory Department, Fritz-Haber-Institute of Max-Planck-Institute

SENCOND REVIEWER

Professor Jürgen P. Rabe
Professor (C4) for the Physics of Macromolecules at the Department of Physics. Humboldt University Berlin

Abstract

This thesis presents an experimental and theoretical study of the structural and electronic properties of carbon nitrides.

Multiple synthesis pathways of carbon nitride were attempted, starting from various precursors under different conditions. XRD, DSC, TGA *etc.* were used to understand the polymerization pathways. In parallel, density functional theory (DFT) calculations were performed in order to study the details of the thermal condensation mechanisms.

The crystal structure of the condensed carbon nitride was studied by the XRD and HRTEM methods and these measurements show two characteristic lattice periodicities: 6.75 Å and 3.26 Å. DFT calculations for two different graphitic crystal structures: g – C_3N_4 and g – C_6N_8 and a previously suggested 3D-structure 3D – C_3N_4 were performed. In addition, we have proposed a new three dimensional structure 3D – C_6N_8, which has lower energy than all phases of carbon nitride published so far. The total energy calculations suggest that $3D - C_6N_8$ is the most stable form among these four carbon nitrides. However, the difference of the cohesive energies between different phases are relatively small, so the other phases may also exist in the crystal structure.

The calculated crystal parameters of these four structures suggest that $g - C_6N_8$, which has an inplane hexagon periodicity of 7.1 Å, and a layer distance of 3.0 Å, is in best agreement with the experimental data.

The measured and calculated polymerization diagrams show a qualitative agreement. The polymerization diagrams reveal that the formation of melem from the precursor is an exothermal reaction. The following reaction steps forming the crystaline carbon nitride are endothermal and the calculations furthermore suggest that the melamine intermediate favors to form the $g - C_6N_8$ phase which has a lower internal energy.

The calculated heat of formations suggest that carbon nitrides are only metastable with respect to nitrogen gas and graphite. This suggests that carbon nitride could decompose forming new nanoporous carbon. Finally, the applications of carbon nitride as catalyst support were investigated experimentally. Different pathways were followed by mixing C_xN_y precursors.

intermediate structures, or the ready-made g-C_xN_y with metal salts. Heat treatment of these materials with the metal salts yields in a partial destruction of the structures, due to oxidation of the organic material. Photoluminescence and excitation spectra indicate a strong interaction of the cyamellur cores with the metal ions, which could be explained by a complexation of the metal ions in the voids of the C_xN_y layers.

Contents

List of Figures

List of Tables

Chapter 1

Introduction

1.1 Motivation

In principle, all binary carbon-nitrogen compounds can be considered as carbon nitrides. They are comprised of an alternating arrangement of carbon and nitrogen atoms, i.e. they do not contain any C-C and/or N-N bonds (with very few exceptions). Many nitrogen-rich organic compounds are characterized by very good oxidative as well as thermal stability. Because of the relatively high electronegativity of nitrogen atoms causes a partial oxidation of the carbon atoms. Oxidation reactions are therefore less likely for nitrogen rich C/N compared to other organic compounds such as hydrocarbons.

The C/N materials described in the literature [1] show in part highly interesting chemical, mechanical, tribological and other functional properties, independent of the preparative procedure, the chemical structure and the composition.

Examination of the optical and electrical properties of C/N-coatings indicated that these materials can be completely transparent, which corresponds well with the theoretically predicted large band gap [2] [3]. Furthermore, a high electrical resistance and a low dielectric constant were measured for amorphous C/N-films [4].

Many carbon nitride coatings were characterized by good corrosion resistance, low coefficient of friction and excellent resistance to wear [5] [6].

This research was initiated and propelled by speculations that saturated (sp^3-hybridised) carbon(IV) nitride phases should be as hard or even harder

than diamond, causing excitement. Theoretical calculations predicted the diamond-like $\beta - C_3N_4$ similar hardness and lower compressibility than diamond. Carbon nitride is among the most promising and most popular compounds to extend the application of carbon in material science.

1.2 Experimental work concerning C_xN_y phases

A number of approaches of the synthesis of new modifications were carried out, due to its extraordinary prospects e.g. as catalyst support. In 1990, Wixom tried to synthesis a carbon(IV) nitride by shock wave compression of a pyrolysed melamineformaldehyde resin and a tetrazol derivative. Diamond was the only detectable crystalline phase in the product[7]. Kouvetakis *et al.* developed a single source precursor route to $g - C_3N_4$ (see Figure 1.1). The pyrolysis products contained small amounts of tin[8]. Recently, Lu *et al.*[9]

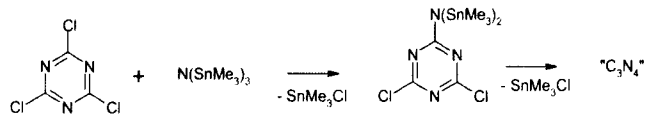

Figure 1.1: Pyrolysis of cyanuric chloride

tried to reproduce the solvothermal carbon nitride synthesis using cyanuric chloride with lithium amide as reactants in benzene solution at 350 °C/5-6MPa (see Figure 1.2). One further attempt to synthesize triazine-based

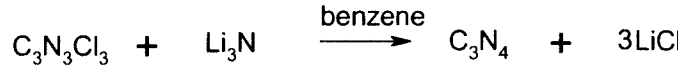

Figure 1.2: Solvothermal reaction of cyanuric chloride with NH_4Cl

graphitic C_3N_4-structures from melamine and cyanuric chloride was reported by Zhang *et al.* in 2001[10]. At 1-1.5 GPa and 500-550 °C, a crystalline phase was obtained, (see Figure 1.3) which contains stoichiometric amounts of HCl. The phase can be considered as a C_3N_4 derivative. Preparation of graphitic

Figure 1.3: High-pressure synthesis of graphitic carbon nitride

C_3N_4 materials based on the tri-s-triazine nucleus C_6N_7 by chemical synthesis

at ambient pressure was reported in 2001 by Komatsu *et al.* [11]. This is a very interesting approach (see Figure 1.4) since it has been demonstrated by *ab initio* calculations that this is the most stable C_xN_y modification[12].

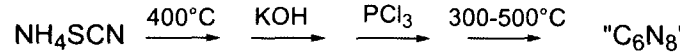

Figure 1.4: Ambient-pressure synthesis of graphitic carbon nitride

1.3 Theoretical work concerning C_xN_y phases

A number of carbon(IV) nitride phases have been theoretically predicted or intuitively suggested by several authors in the literature. Guo and Goddard were the first to investigate a carbon(IV) nitride phase (see Figure 1.5) in analogy to the very well-known $\alpha - Si_3N_4$[13]. The structure can be described as an AB-stacking of undulated $\beta - C_3N_4$ layer. The carbon atoms are tetrahedral coordinated with nitrogen atoms. The corner-sharing tetrahedra form a covalent network of three-, four- and six-member rings.

Liu and Cohen proposed $\beta - C_3N_4$ (see Figure 1.6) by using the same

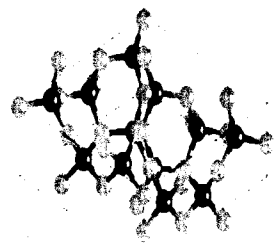

Figure 1.5: $\alpha - C_3N_4$

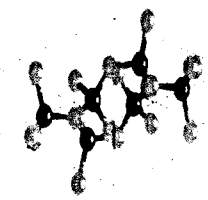

Figure 1.6: $\beta - C_3N_4$

relative positions of the atoms in the β silicon nitride phase and replaced the Si-N bond by the shorter C-N[14]. A possible pyramidal arrangement around the nitrogen atoms was not taken into account. Similar to the α phase, the carbon atoms are tetrahedrally coordinated by nitrogen atoms.

Kroll and Hoffmann discovered a new and unusual C_3N_4 solid state structure:

$\gamma - C_3N_4$ (see Figure 1.7). This phase consists of tetrahedrally coordinated carbon atoms and both three-fold, planar, and pyramidal coordinated nitrogen atoms. In contrast to the other phases mentioned here, this structure contains C-C and N-N bonds[15].

According to Teter and Hemley[16], when tri-s-triazine rings are connected

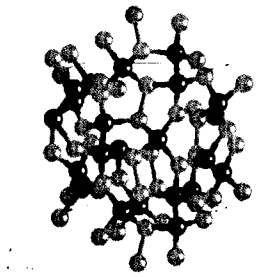

Figure 1.7: $\gamma - C_3N_4$

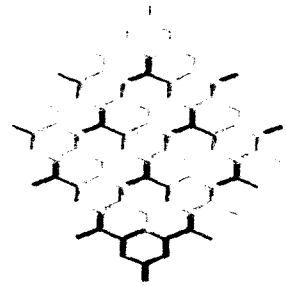

Figure 1.8: $g - C_3N_4$

via trigonal planar coordinated nitrogen atoms, layered structures can be designed (see Figure 1.8), which are similar to graphite in the sense that they should be planar and aromatic with (at least partially) delocalized π-electrons. However, the layers contain "holes" filled by electrons in the non-bonding sp^2-orbitals of the nitrogen atoms in the s-triazine rings.

Vodak *et al.* investigated "3D-srs" and "3D-ths" (see Figure 1.9,1.10), which are derived from $SrSi_2$ and $ThSi_2$ structures[17]. In this case s-triazine units may be connected via nitrogen atoms to form 3D-networks. DFT calculations indicated that the 3D arrangements are more stable than the layered systems. This is a consequence of the lone-pair repulsion of the non-bridging triazine nitrogen, which would be in close vicinity to each other in coplanar structures.

Other stoichiometries of carbon nitrides were also considered. In Mattesini' paper [18], they investigated the different structures of carbon nitrides with C_11N_4 stoichiometry. These phases contain less than 30% of nitrogen than the well-known C_3N_4 phase. We propose that lowering the nitrogen concentration does not prevent finding new ultrahard materials and indeed bring a significant increase in the cohesive energies of carbon nitrides. However, the calculated enthalpies of formation are positive and generally greater than those of their carbon-deficient counterparts.

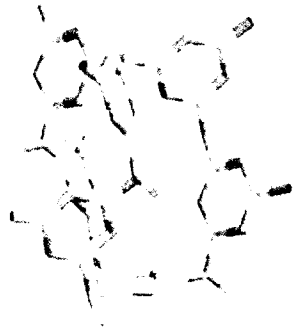

Figure 1.9: $3D - srs$

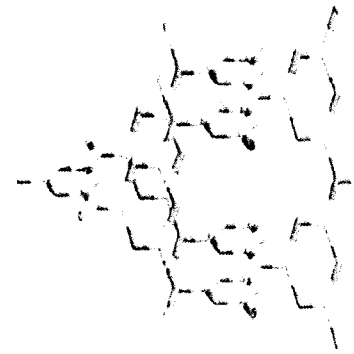

Figure 1.10: $3D - ths$

Carbon nitride with 1:1 stoichiometry has been examined by Michel's group [19]. They used the general valence rule (detail discussion in section 3.3) to state the requirements of semiconductor or an insulating structure for this compound. They indicated that C_3N_4 is an important stable stoichiometry for carbon nitride.

1.4 Aim for Master Thesis

At this stage, it is not clear which is the most stable structure of carbon nitride. In this thesis, the experimental and theoretical methods are combined to determine and rationalize the stable form of carbon nitride. The experimental study focuses on investigating various synthesis pathways of carbon nitride from different monomer under different conditions. Density functional calculations were carried out with the aim to explain the experimental observations and to gain further understanding of the polymerization schemes using thermodynamic theories. The theoretical investigations also provided an useful approach to develop the application of carbon nitride materials.

Chapter 2

Experimental Work

Recently, it was reported that cyanamide and dicyanamide can be used as monomers to form $g - C_xN_y$. By a simple self-condensation process, these monomers form a material that consists of condensed cyamellur/C_6N_7-units. During the master work, the use of $g - C_xN_y$ as catalyst support was exploited. Different pathways to complex metals with high catalytic activity, such as palladium or platinum, were investigated and the resulting composite materials were analyzed by means of TGA, WAXS, TEM and photoluminescence spectroscopy.

2.1 Synthesis of Carbon Nitride

2.1.1 From cyanamide/dicyandiamide

Experiment

Cyanamide / dicyandiamide were calcined in tight but not sealed steal tubes using a programmable muffle type furnace. For $g-C_xN_y$, the monomers were calcined at 550 °C for four hours, with an applied heating rate of 5 K/min. Polymeric C_xN_y ($p-C_xN_y$), characterized by an incomplete condensation of the cyamellur cores, was made by calcinations of the monomer at 400 °C for 4 h.

Result

Thermalanalysis methods(TGA,DSC) in combination with XRD are used to characterize the intermediate steps along the condensation of the molecular monomers into carbon nitride. As shown in Figure 2.1 and table 2.1, at 47 °C

cyanamide melts and dimerizes to dicyandiamide which has finishes at about 160 °C. Followed by the exothermic trimerization reaction into melamin, which take place at 240 °C. The melamine starts to sublimate at around

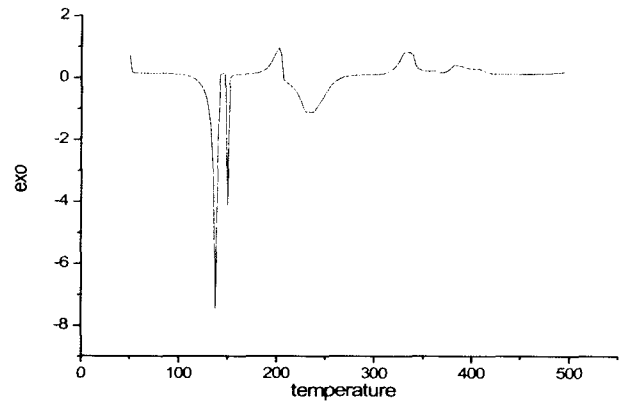

Figure 2.1: DSC thermogram for formation of carbon nitride from cyanamide

340 °C. At about 380 °C, the cyameluric nucleus forms out of 3 melamine units, as already reported by Schnick *et. al.* in the synthesis of melem[20]. The melem itself undergoes further condensation. Due to the open system,

Table 2.1: Transitions identified by DSC

Temperature	Relate process
47 °C	Melting point(mp) of cyanamide
137 °C	Reaction of cyanamide into dicyandiamide
203 °C	mp of dicyandiamide
234 °C	Reaction of dicyandiamide into melamine
335 °C	Sublimation point(sp) of melamine
389 °C	Formation of cyameluric core out of melamine
525 °C	Formation of carbon nitride network

the polymerization processing is always pure in ammonia at ambient pressure, which shift the equilibrium to the more condensed polymeric species. Further heating of this species results in further elimination of ammonia and the formation of practically condensed C_xN_y network at around 500°C. The

proposed polymerization scheme is shown in Figure 2.2.

The WAXS pattern of $g - C_xN_y$ condensed at 550 °C shows two peaks

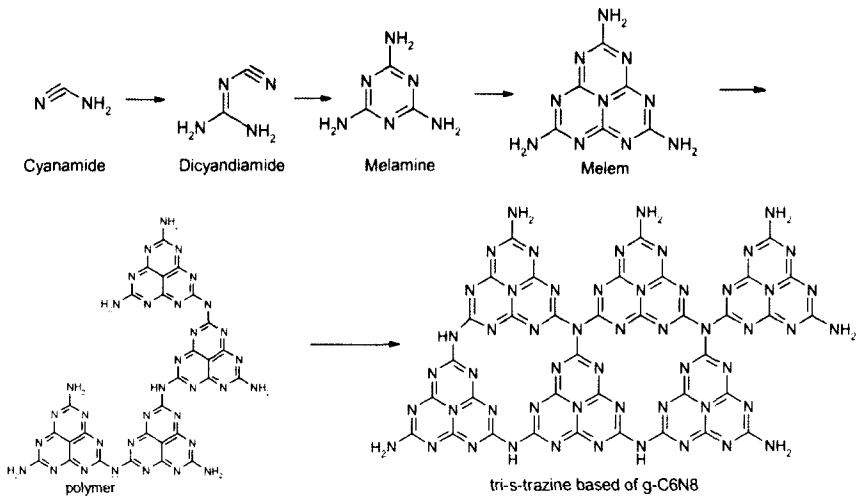

Figure 2.2: Proposed polymerization pathway of carbon nitride

(see Figure 2.3). The more intense peak at 27.7 °C could be identified as the (002) peak of $g - C_xN_y$ which corresponds to a stacking distance of the aromatic units of d = 0.326 nm. Another peak at 13.1 °C which corresponds to a d-value of 0.675 nm indicates the in-plane periodicity of the cyammellur cores and the resulting voids.

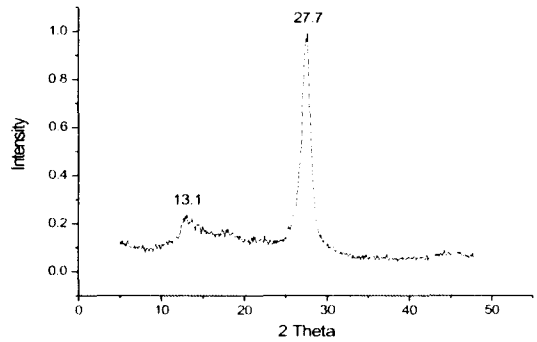

Figure 2.3: XRD pattern of $g - C_xN_y$ from cyanamide/dicyandiamide

2.1.2 From pyrazine

Experiment

Solid monomers, like phtalocyanines, were calcined in the same way as described in (1) Pyrazine carbonitrile (PCN) was heated in tight but not sealed tubes in a sand bath covering one quarter of the tube. The sand bath was heated at different temperatures for 4 h.

Result

Because of the low boiling point of pyrazine carbonitrile (bp=200 °C), pyrolysis of the monomer cannot be performed using the above described method. To prevent complete evaporation of the monomer, the tight but not sealed steal tubes were heated in a sand bath covering one quarter of the tube, ensuring a temperature gradient along the tube. Evaporated monomer is condensed on the top of the tube and then transported back to the bottom.

To investigate the polymerization process, a series of temperatures were carried out in the sand bath. Samples were heated at 400 °C,450 °C,500 °C and 550 °C for 4 h, respectively. The temperatures and description of the products are shown in table 2.2.

The structural changes at different temperatures were studied by tempera-

Table 2.2: Products at different temperature

Temperature/°C	350	400	450	500	550
Color/ Appearance	Purple viscous liquid	White needles	Darkgray powder	Dark gray powder	Light gray powder

ture dependent WAXS experiments (see Figure2.4). At lower temperatures, sharp peaks at lower angles indicate a crystalline arrangement of smaller organic molecules. Note that the XRD pattern as well as the appearance of the product (white needles), indicate the formation of a single and well defined compound, leading to a possible "high temperature organic chemistry". Elemental analysis reveals the composition of this compound as $C_5N_3H_3$ - which is exactly the composition of pyrazine carbonitrile. A possible explanation (see Figure 2.5) of this consistency in the elemental analysis would be a trimerization of the pyrazine carbonitrile.

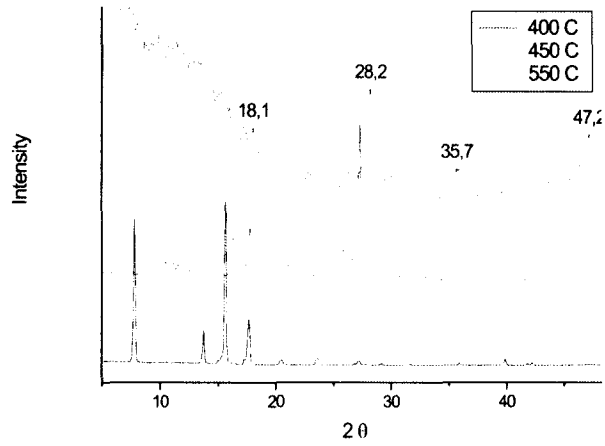

Figure 2.4: XRD of heating pyrazine carbonitrile at different temperature

The peaks at smaller angles disappear at 450°C, while an intense peak

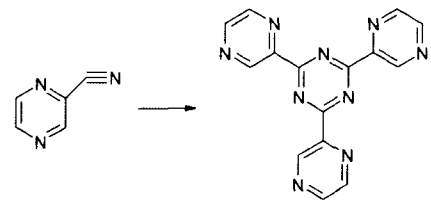

Figure 2.5: Possible polymerization of pyrazin carbonitrile

at 27.3° emerges. Like $g - C_xN_y$, this is usually identified as the (002) peak of graphitic structures and corresponds to a stacking distance of aromatic units of d = 0.326 nm. At a higher temperature (550°C), shifts to larger angles were observed, corresponding to the shortening in the stacking distance of the layers (d = 0.316 nm). This distance represents an astonishing small value for the packing of aromatic units. Unfortunately, due to the low yield of the product, no further characterization, like elemental analysis, could be carried out.

The micrograph reveals the existence of two species in the material. The major part of the material (see Figure 2.6) consists of small crystallites of

Figure 2.6: TEM of major product of pyrazine carbonitrile heated to 550°C

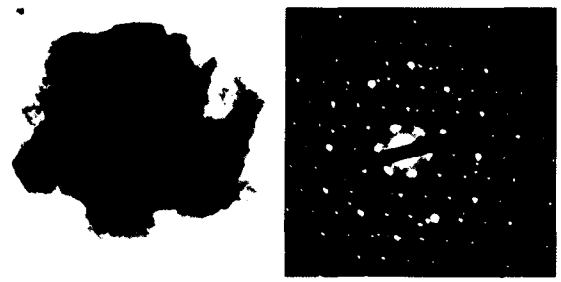

Figure 2.7: TEM of minor product pyrazine carbonitrile heated to 550°C

around 50 nm in diameter, yielding a polycrystalline electron diffraction pattern, while the minor part of the sample (see Figure 2.7) consists of larger single crystals of several micrometers in diameter, which are arranged in a layer-like structure.

The corresponding d-spacing from the electron diffraction pattern are shown in table 2.3. In conclusion, pyrazine carbonitrile was heated and the prod-

Table 2.3: $d-spacing$ resolved from diffraction pattern

Number of circle i	1	2	3	4	5	6
Correspond length L_i / Å	4.7	2.7	2.4	1.8	1.6	1.3
Ratio of L_l/L_i	1	$\sqrt{3}$	2	$\sqrt{7}$	9	$\sqrt{13}$

ucts at different temperatures were analyzed by means of XRD and TEM. Although the yields were low and therefore further analysis of the products was impracticable, pyrazine carbonitrile shows a high potential to form new

carbon nitride.

2.2 Graphitic C_xN_y as catalyst support

Due to its unique structure, combining high-density surface and multiple inclusion sites, $g - C_xN_y$ is a promising support for metals. In this chapter, the intercalation and complexation of palladium and platinum at $g - C_xN_y$ were examined. Three different approaches were used in this progress:
One step approach: The C_xN_y-precursor was heated in the presence of metal salt to directly form the C_xN_y network incorporated metal ions

Two step approach: The $g - C_xN_y$ support was synthesized in the first step, followed by the incorporation of the metal salt in solution

Three step approach: At first, a polymeric $C_xN_yH_x$ was synthesized, which was subsequently used as ligand for the complexation of the metal ions in solution. In the last step, the complex is heated to form the g-C_xN_y network.

2.2.1 One step approach

Experiment

Different ratios (see table 2.4) of dicyandiamide and $PdCl_2$ were well mixed and heated in a tight but not sealed steal tube using a programmable muffle type furnace. The mixture was calcined at 550°C for four hours, with an applied heating rate of 5 K/min.

Table 2.4: Experiment details of one step approach

Ratio	3 : 1	6 : 1	12 : 1	24 : 1
m(dicyandiamide)/g	0.043	0.057	0.057	0.110
m($PdCl_2$)/g	0.030	0.020	0.010	0.010

Result

The XRD analysis (see Figure 2.8) of the heated mixtures reveals a crucial influence of the dicyandiamide/$PdCl_2$-ratio on the resulting product. This is due to a partial oxidation of the monomer by the metal salt, proved by the sharp peaks at 40.2° and 46.5°, which correspond to the pure palladium metal. At higher molar ratios (dicyandiamide:Pd = 24:1), adequate amount

of monomer material remain to form the graphitic C_xN_y. At lower ratios, the oxidation of the organic material becomes the dominating reaction, avoiding the formation of the $g - C_xN_y$ structure. The formation of g-C_xN_y at high ratios is expressed by the peak at 27.5°, which shows interlayer distance of the structure. Interestingly, for lower values some new peaks can be identified in the XRD-pattern. A sharp, but not very intense peak at 26.0° at an

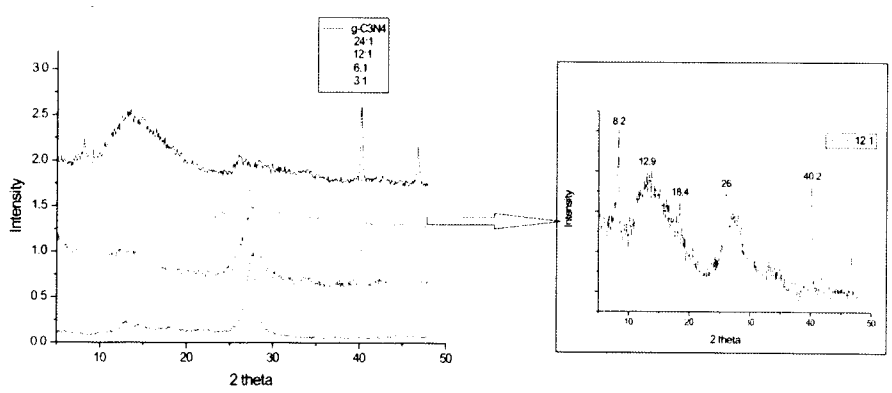

Figure 2.8: XRD of different ratio of dicyandiamide:$PdCl_2$(left) Ratio= 12 : 1(right)

intermediate ratio (dicyandiamide:Pd = 12:1) indicates a partial formation of a layer-like structure, while the interlayer distance shows a significant increase from 3.24 Åto 3.42 Å, probably due to inclusion of the metal. Two additional peaks at 8.13° and 18.2° (d = 10.9 Å and 4.8 Å) can be further identified (note that the d value (4.8 Å) is also found in a crystalline "all carbon" - side product of the pyrolysis of dicyandiamide to C_xN_y. Therefore, heat treatment of cyanamide with the palladium salt might be a promising approach to increase the yield of this side product.)

2.2.2 Two step approach

Experiment

a) Bulk $g - C_xN_y$ + metal salt (s)
Different ratios (table 2.5) of the bulk $g - C_xN_y$ and $PdCl_2$ were well mixed

and heated in a tight but not sealed steal tube using a programmable muffle type furnace. The mixture was calcined at 550°C for four hours, with an applied heating rate of 5 K/min.

Table 2.5: Experiment details of 2 step approach a

Ratio	1 : 1	2 : 1	4 : 1	10 : 1
m$(g - C_xN_y)/g$	0.03	0.03	0.04	0.11
m$(PdCl_2)/g$	0.03	0.015	0.01	0.01

b) Bulk $g - C_xN_y$ + metal salt (l)
0.02 g $g - C_xN_y$ was added to a solution of K_4PtCl_2 (0.06g) in 5mL water (molar ratio Pt:cyamellur-unit is 1:1). The mixture was parted into three vials and the samples were stirred for 24 hours at different temperatures (RT, 60°C, 80°C).

c) Nano $g - C_xN_y$ + metal salt (l)
0.03 g nano-$g - C_xN_y$ was added to a solution of $PdCl_2$ (0.03g) in 5mL concentrated HCl (molar ratio Pd:cyamellur -unit 1:1). The solution was stirred for 24 hours at room temperature.

Result

a) Bulk $g - C_xN_y$ + metal salt (s)
For the last set of experiments, the condensed graphitic-C_xN_y was used as

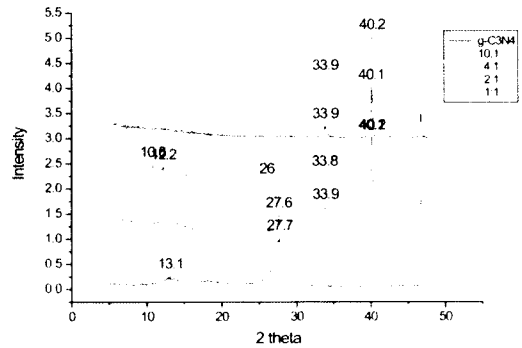

Figure 2.9: XRD of different ratio of $g - C_xN_y$: $PdCl_2$

support for the metal salts. In the first experiment C_xN_y was mixed with the metal salt and heated to 550°C. A general conclusion of these experiments is that the graphitic C_xN_y structure is just preserved at a maximum support/metal-ratio of around 10:1. Higher amounts of the metal salts are needed to destroy the graphitic structure or disturb the formation of it, due to the oxidation of the organic compounds. Note that the XRD curves in Figure 2.9 show an additional peak at 33.6° corresponding to a d-value of 2.64 Å, which cannot be assigned to $g - C_xN_y$, Pd or $PdCl_2$.

b) Bulk $g - C_xN_y$ + metal salt (l)
Considering the above experiments, the most promising approach towards C_xN_y /metal composites is the intercalation of metal salts from solution. This approach has the advantage that no further heat treatment of the composites is necessary. Reduction of the metal ions can be carried out by gentle methods like treatment with hydrogen gas. On the other side, a major disadvantage of this approach might be the inefficient infiltration of the dense, layer-like structure of $g - C_xN_y$. Therefore the major focus of this study was to find a way for an efficient loading of metal ions into $g - C_xN_y$.

Because water was used as solvent in all experiments, in a reference ex-

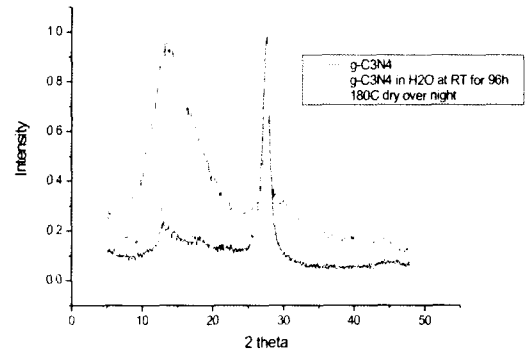

Figure 2.10: Influence of water on $g - C_xN_y$

periment the influence of water on the structure of $g - C_xN_y$ was exploited. Figure 2.10 shows the influence of pure water on $g - C_xN_y$. After 180° heat treatment overnight, compare the $g - C_xN_y$ as prepare (black) and dry sample after stirring 96 hours in pure water (green), no change of the structure is obtained. Compare the curve before (red) and after (green) drying process,

the first broad peak around 13.1° change to a lower intensity. So a thorough drying of the material is necessary.

Figure 2.11 shows the XRD patterns of $g - C_xN_y$ stirred in solutions of

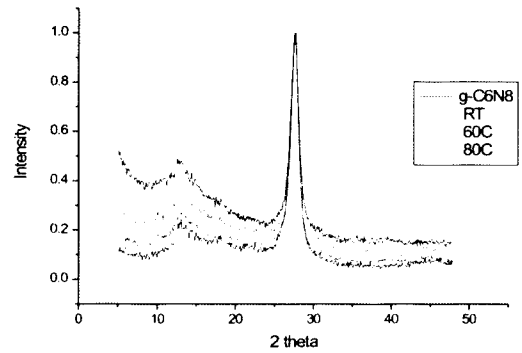

Figure 2.11: Carbon nitride $+K_4PtCl_2$ in solution at different temperature

K_2PtCl_6 with constant concentration at different temperatures. No significant changes are observed, except a small increase in the intensity of the peak at lower angles, corresponding to the void-void distance in the layers. That could be explained by an incorporation of metal ions into the voids. This incorporation should affect the intensity of this peak, due to the associated higher electron density for these periodicities. Anyhow, this result does not necessarily prove an incorporation of metal ions.

A much better indication is given by thermal gravimetrical analysis (TGA) of the materials. Table 2.6 summarizes the remaining mass after heat treatment. Obviously the incorporation of the metal ions is more effective when

Table 2.6: Mass remaining after heat treatment

Temperature/°C	25	60	80
Ratio of remaining mass	0.86%	4.37%	5.64%

it is carried out at higher temperatures. The highest amount of remaining mass is reached at 80°C and gave a mass of 5.64%. Considering the mass of K_2PtCl_6, this corresponds to a C_6N_8/Pt ratio of approximately 44:1. Thus, every forty fourth void is complexing one Pt-ion. Even though these ratios are comparatively small, there is little doubt that the amount of metal ions

can be further increased, for example by using longer reaction times.

The position of the included metal ions is a further point of interest. Different binding situations of the metal ions in the C_xN_y structure are possible: First, a non selective binding, i.e. inclusion of the metal salts between the carbon nitride layers is possible, comparable to the intercalation of metal salts into the layers of graphite. Another possibility is the above mentioned complexation of the metal salts in the voids of the C_xN_y materials, which have a related structure to well known ligands like porphyrine or phtalocyanine. The position of the metal ions in this case should therefore rather be described as "in" the layer than "between" the layers.

Indication about the binding state can be achieved by photoluminescence

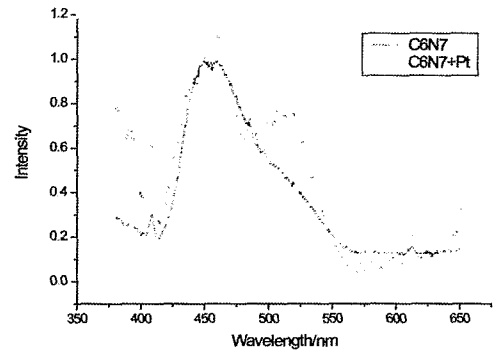

Figure 2.12: Photoluminescence spectroscopy at $\lambda = 340$ nm

spectroscopy. Figure 2.12 shows the photoluminescence spectra of pure C_xN_y and C_xN_y with included metal salts. Pure C_xN_y exhibits a single peak at lmax = 456 nm. For the composite material, a second peak at lmax = 514 nm appears, indicating two energy states of the cyamellur cores. This can be attributed to a strong interaction of the metal ion with the support, indicating a complexation of the metal ions.

Excitation spectra (see Figure 2.13) confirm this result. It can be seen that the two emission peaks in the PL spectrum originate from two different species. Considering that in the excitation spectra of pure C_xN_y, only the higher energy form (i.e. the excitation band at lower wavelength) exist, this can be attributed to a shortening of the HOMO-LUMO distance in the

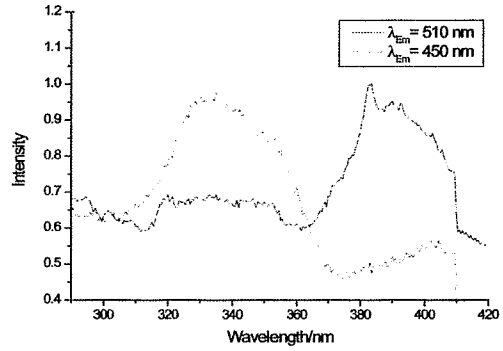

Figure 2.13: Excitation spectra of C_xN_y + Pt

cyamellur cores due to complexation of the metal salt.

c) Nano $g - C_xN_y$+ metal salt (l)
Recent work of the inclusion of perfluorinated carboxylic acids in C_xN_y showed that a much more efficient inclusion is possible, when g-C_xN_y nanoparticles are used as support rather than the bulk material.

Thus, one experiment using g-C_xN_y nanoparticles (diameter = 50-70 nm)

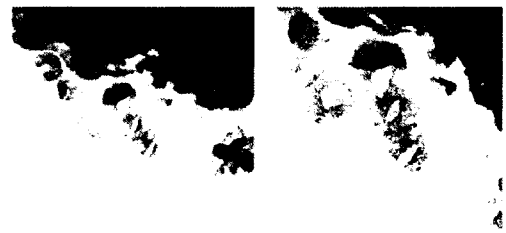

Figure 2.14: TEM of nanoparticles carbon nitride

instead of the bulk material was carried out. The nanoparticles are synthesized by a casting/replication approach (details are described in the literature). TEM micrographs of nanoparticles are shown in Figure 2.14.

The XRD patterns of the g-C_xN_y nanoparticles (see Figure 2.15) before

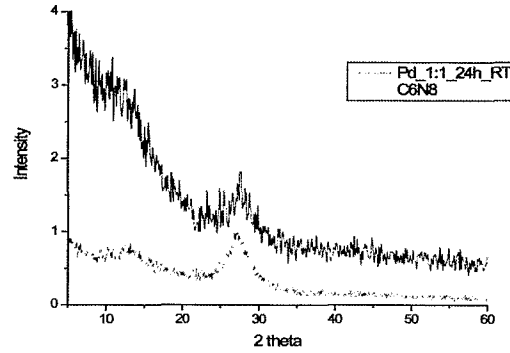

Figure 2.15: XRD of complex metal in nano-carbon nitride

and after complexation of the metal ions show no significant differences. After stirring of nano-C_xN_y in a $PdCl_2$/Acetonitrile solution for 24 h at room temperature an incorporation of 15.4% mass of $PdCl_2$ could be observed, by means of TGA. Considering the mass of $PdCl_2$, this corresponds to a C_6N_8/Pd^{2+} ratio of approximately 5:1.

The same inclusion conditions for a bulk material yield in an incorporation of 0.86% mass $PdCl_2$, which clearly proves the advantage of nanostructured morphology of the carbon nitrides for inclusion experiments.

2.2.3 Three step approach

Experiment

a) Polymer + metal salt (l)
0.02 g of the $C_xN_yH_x$ polymer was added to a solution of K_4PtCl_2 (0.06g) in 5mL water. The mixture was stirred at room temperature for 96 hours, filtered, washed several times with water and ethanol and subsequently dried. The polymer metal complexes were calcined in tight but not sealed steal tubes at 550°C for four hours, with an applied heating rate of 5 K/min.

b) Polymer + metal salt (s)
Different ratios (see table 2.7) of dicyanamide and $PdCl_2$ were well mixed

and heated in a tight but not sealed steal tube using a programmable muffle type furnace. The mixture was calcined at 550°C for four hours, with an applied heating rate of 5 K/min.

Table 2.7: Experiment details for 3 steps approach b

Ratio	5 : 1	10 : 1	20 : 1
m(polymer)/g	0.05	0.11	0.21
m($PdCl_2$)/g	0.01	0.01	0.01

Result

As shown above, oxidizing metal salts have a crucial effect on the formation of g-C_xN_y when they are added to the monomer during pyrolysis. On the other hand, the dense structure of fully condensed g-C_xN_y might avoid an effective inclusion of the metal salts, as it was shown for the inclusion of perfluoro carboxylic acids [21].

Considering this, an intermediate, polymeric melem, which is formed from dicyandiamide at 400°C (see the 4th step in Figure 2.2), was used for the complexation and inclusion experiments.

a) Polymer + metal salt (l)
Different ratios of the polymer and $PdCl_2$ were well mixed and subsequently

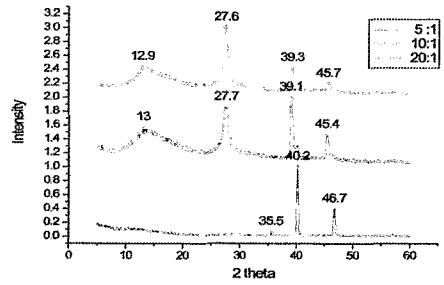

Figure 2.16: XRD of different ratio of polymer/$PdCl_2$

heat treated. The XRD-pattern (see Figure 2.16) shows similar result as the

monomer/polymer mixtures. The polymer seems to possess a higher acceptance to metal salts during heat treatment compared to dicyandiamide. The graphitic structure is still obtained at C_xN_y/Pd weight ratios of 10:1.

b) Polymer + metal salt (s)
The polymer was added to the water solution of K_4PtCl_2 and stirred for

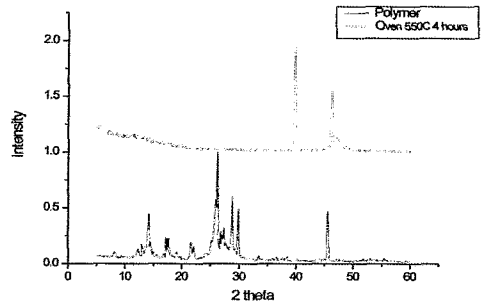

Figure 2.17: XRD of complex metal on polymer in solution 96 hours at R.T.

96 hours. After filtration and washing, the solid was heated to 550°C for 4 hours. Figure 2.17 shows the X-ray diffraction pattern of the polymer before and after complexation with metal salt and subsequent heat treatment. The resulting material (green curve) shows no indication of a formed g-C_xN_y structure, instead the characteristic pattern for metallic platinum is observed. Again, this can be explained by an oxidation of the polymer from the metal salt during the heat treatment. Even though the desired structure of the carbon nitride was not obtained, this experiment gives a clear indication of the strong complexation ability of the polymer to the platinum salt. As shown in the previous experiment, a relatively high amount of the platinum salt (5:1) is needed to completely disturb the formation of g-C_xN_y. At least this amount of platinum ions must have been separated from the solution via complexation by the polymer.

2.3 Conclusion

In the first set of experiments, pyrazine carbonitrile was introduced as new monomer for carbon nitride materials. TEM result suggests that heat treatment of this monomer yields two different crystalline species. Temperature dependent XRD experiments show the transformation of liquid PCN at room temperature to a well defined organic crystal at 350°C. By increasing the temperature up to 550°C, a graphite analogous structure is formed.

In the second set of experiments, g-C_xN_y was successfully used as support for metal ions such as Pd^{2+} and Pt^{4+}. Different pathways were followed by mixing C_xN_y monomers, intermediate structures, or the ready-made g-C_xN_y with metal salts. Heat treatment of these materials with the metal salts yields in a partial destruction of the structures, due to oxidation of the organic material. Mixing bulk g-C_xN_y with metal salts in solution, partially incorporated metal ions could be formed. As one crucial parameter, for the amount of included salt, the reaction temperature was identified. Photoluminescence and excitation spectra indicate a strong interaction of the cyamellur cores with the metal ions, which could be explained by a complexation of the metal ions in the voids of the C_xN_y layers.

Future works will focus on the use of the carbon nitride-metal compounds for catalysis, as well as investigation of structure and properties of new carbon nitrides.

Chapter 3

Theoretical Work

3.1 Background

3.1.1 The Schrödinger Equation of solid

[22] The ultimate goal of most quantum chemical approaches is the - approximate - solution of the time-independent, non-relativistic Schrödinger equation

$$\hat{H}\Psi_i(\vec{x}_1, \vec{x}_2, ..., \vec{x}_N, \vec{R}_1, \vec{R}_2, ..., \vec{R}_M) = E\Psi_i(\vec{x}_1, \vec{x}_2, ..., \vec{x}_N, \vec{R}_1, \vec{R}_2, ..., \vec{R}_M) \,. \tag{3.1}$$

where $\hat{H}$ is the Hamilton operator for a molecular system consisting of M nuclei and N electrons in the absence of magnetic or electric fields. $\hat{H}$ is a differential operator representing the total energy:

$$\hat{H} = -\frac{1}{2}\sum_{i=1}^{N}\nabla_i^2 - \frac{1}{2}\sum_{I=1}^{M}\frac{1}{M_I}\nabla_I^2 - \sum_{i=1}^{N}\sum_{I=1}^{M}\frac{Z_I}{r_{iI}} + \sum_{i=1}^{N}\sum_{j>i}^{N}\frac{1}{r_{ij}} + \sum_{I=1}^{M}\sum_{J>I}^{M}\frac{Z_I Z_J}{R_{IJ}} \tag{3.2}$$

Here, I and J run over the M nuclei while i and j denote the N electrons in the system. The first two terms describe the kinetic energies of the electrons and nuclei, respectively. M_I is the mass of nucleus I in multiples of the mass of an electron (atomic unit, see table 3.1). The remaining three terms define the potential part of the Hamiltonian and represent the attractive electrostatic interaction between the nuclei and the electrons and the repulsive potential due to the electron-electron and nucleus-nucleus interactions, respectively. r_{ij} (and similarly R_{IJ}) is the distance between the particles i and j, i. e., $r_{ij} = |\vec{r}_i - \vec{r}_j|$. $\Psi_i(\vec{x}_1, \vec{x}_2, ..., \vec{x}_N, \vec{R}_1, \vec{R}_2, ..., \vec{R}_M)$ stands for the wave function of the i*th* state of the system, which depends on 3N spatial coordinates $\vec{r}_i$, and N spin coordinates s_i of the electrons, which are collectively termed $\vec{x}_i$, and

Table 3.1: Atomic units

Quantity	Atomic unit	Value in SI units	Symbol
mass	rest mass of electron	$9.1094 \cdot 10^{-31}$ kg	m_e
charge	elementary charge	$1.6022 \cdot 10^{-19}$ C	e
action	Planck's constant/2π	$1.0546 \cdot 10^{-34}$ Js	$\hbar$
energy	$\hbar/m_e a_0^2$	$4.3597 \cdot 10^{-18}$ J	E_h(hartree)

3M spatial coordinates of the nuclei $\vec{R}_I$. The wave function Ψ_i contains all information that can possibly be known about the quantum system at hand. Finally, E_i is the numerical value of the energy of the state described by Ψ_i.

3.1.2 Born-Oppenheimer Approximation

There is a significant difference between the masses of nuclei and electrons [22]. Even the lightest nucleus, the proton (^{1}H), weights roughly 1800 times greater than an electron, and for a typical nucleus such as carbon the mass ratio well exceeds 20,000. Thus, the nuclei move much slower than the electrons. The practical consequence is that we can, at least to a good approximation, take the extreme point of view and consider the electrons as moving in the field of fixed nuclei. This is the famous Born-Oppenheimer or clamped-nuclei approximation. Of course, if the nuclei are fixed in space and do not move, their kinetic energy is zero and the potential energy due to nucleus-nucleus repulsion is merely a constant. Thus, the complete Hamiltonian given in equation 3.2 reduces to the so-called electronic Hamiltonian

$$\hat{H}_{elec} = -\frac{1}{2}\sum_{i=1}^{N}\nabla_i^2 - \sum_{i=1}^{N}\sum_{I=1}^{M}\frac{Z_I}{r_{iI}} + \sum_{i=1}^{N}\sum_{j>1}^{N}\frac{1}{r_{ij}} = \hat{T} + \hat{V}_{eI} + \hat{V}_{ee} \tag{3.3}$$

The solution of the Schrödinger equation with $\hat{H}_{elec}$ is the electronic wave function Ψ_{elec} and the electronic energy E_{elec}. Ψ_{elec} is the function of electron coordinates, while the nuclear coordinates enter only parametrically and do not explicitly appear in Ψ_{elec}. The total energy E_{tot} is then the sum of E_{elec} and the constant nuclear repulsion term,

$$E_{nuc} = \sum_{I=1}^{M}\sum_{J>I}^{M}\frac{Z_I Z_J}{r_{IJ}} \tag{3.4}$$

$$\hat{H}_{elec}\Psi_{elec} = E_{elec}\Psi_{elec} \tag{3.5}$$

$$E_{tol} = E_{elec} + E_{nuc} \tag{3.6}$$

The attractive potential exerted on the electrons due to the nuclei-the expectation value of the second operator $\hat{V}_{eI}$ in equation 3.3 is also often termed the external potential $\hat{V}_{ext}$ in density functional theory, even though the external potential is not necessarily limited to the nuclear field but may include external magnetic or electric fields etc. From now on we will only consider the electronic problem of equations 3.3 and 3.6 and the subscript 'elec' will be dropped.

3.1.3 The Variational Principle

What we need to do in order to solve the Schrödinger equation 3.5 for an arbitrary molecule is first to set up the specific Hamilton operator of the target system. To this end we need to know those parts of the Hamiltonian $\hat{H}$ that are specific for the system at hand. In the second step we have to find the eigenfunctions Ψ_i and corresponding eigenvalues ϵ_i of $\hat{H}$. Once the Ψ_i are determined, all properties of interest can be obtained by applying the appropriate operators to the wave function. Unfortunately, this simple and innocuous-looking program is of hardly any practical relevance, since apart from a few, trivial exceptions, no strategy to solve the Schrödinger equation exactly for atomic and molecular systems is known.

Nevertheless, the situation is not completely hopeless. There is a recipe for systematically approaching the wave function of the ground state Ψ_0, the state which delivers the lowest energy E_0. This is the variational principle, which holds a very prominent place in all quantum-chemical applications. The variational principle states that the expectation value of the Hamilton operator $\hat{H}$ from any guessed Ψ_{trial} will be an upper bound to the true energy of the ground state,

$$< \Psi_{trial}|\hat{H}|\Psi_{trial} >= E_{trial} \geq E_0 =< \Psi_0|\hat{H}|\Psi_0 > \tag{3.7}$$

where the equality holds if and only if Ψ_{trial} is identical to Ψ_0.

The strategy for finding the ground state energy and wave function should be clear by now: we need to minimize the functional E[Ψ] by searching through all acceptable N-electron wave functions. The wave function which gives the lowest energy will be Ψ_0 and the energy will be the true ground state energy E_0. This recipe can be compactly expressed as

$$E_0 = \min_{\Psi \to N} E[\Psi] = \min_{\Psi \to N} < \Psi|\hat{T} + \hat{V}_{eI} + \hat{V}_{ee}|\Psi > \tag{3.8}$$

where $\Psi \rightarrow$ N indicates that Ψ is an allowed N-electron wave function.

Let us summarize what we have shown so far: once N and V_{ext} (uniquely determined by Z_I and R_I) are known, we can construct $\hat{H}$. Through the prescription given in equation 3.8 we can then - at least in principle - obtain the ground state wave function, which in turn enables the determination of the ground state energy and of all other properties of the system. Pictorially, this can be expressed as

$$N, Z_I, R_I \Rightarrow \hat{H} \Rightarrow \Psi_0 \Rightarrow E_0$$

Thus, N and V_{ext} completely and uniquely determine Ψ_0 and E_0. We say that the ground state energy is a functional of the number of electrons N and the nuclear potential V_{ext},

$$E_0 = E[N, V_{ext}] \tag{3.9}$$

3.1.4 The Hartree-Fock Approximation

As discussed above, it is impossible to solve equation 3.8 by searching through all acceptable N-electron wave functions. We need to define a suitable subset. In the Hartree-Fock scheme, it consists of approximating the N-electron wave function by an antisymmetrized product of N one-electron wave functions $\chi(\vec{x}_i)$. This product is usually referred to as a Slater determinant Φ_{SD}:

$$\Phi_{SD} = \frac{1}{\sqrt{N!}} det|\chi_1(\vec{x}_1)\chi_2(\vec{x}_2)...\chi_3(\vec{x}_3)| \tag{3.10}$$

$\chi_i(\vec{x}_i)$ are called *spin orbitals*, each of which is composed of a spatial orbital and one of the two spin functions.

The next step is to use the variational principle in order to find the best Slater determinant. E_{HF} is obviously a functional of the spin orbitals. Thus, the variational freedom in this expression is in the choice of the orbitals. Equation 3.11 represent the Hartree-Fock equations, which determine the 'best' spin orbitals, those $\chi_i\vec{x}_i$ for which E_{HF} attains its lowest value.

$$\hat{f}\chi_i = \varepsilon_i\chi_i \tag{3.11}$$

The ε_i have the physical interpretation of orbital energies. The Fock operator $\hat{f}$ is an effective one-electron operator defined as

$$\hat{f}_i = \hat{T} + \hat{V}_{eI} + \hat{V}_{HF}(i) \tag{3.12}$$

where $F[\rho]$ is a universal functional and independent of V_{ext}. For a given V_{ext}:

$$\begin{aligned} E_0[\rho] &= \int \rho(\vec{r}) V_{ext} d\vec{r} + F[\rho] \\ &= \int \rho(\vec{r}) V_{ext} d\vec{r} + < \Psi_0 | T + V_{ee} | \Psi_0 > \end{aligned} \tag{3.18}$$

As the total energy is a functional of the density, it is possible to extract some parts that are obviously density functionals. The remaining parts will be density functional, too.

But how can we be sure that a certain density is really the ground state density that we are looking for? The second theorem states that $F[\rho_0]$, the functional that delivers the ground state energy of the system, delivers the lowest energy if and only if the input density is the true ground state density, $\rho(\vec{r})$. This is of course nothing else than variational principle which in the present context can be expressed as

$$E_0[\rho_0] \leq E_0[\rho] \tag{3.19}$$

Let us summarize. First, all properties of a system defined by an external potential V_{ext} are determined by the ground state density. Second, this functional attains its minimum value with respect to all allowed densities if and only if the input density is the true ground state density.

3.1.7 The Kohn-Sham Approach

In 1965, Kohn and Sham [27] suggested an avenue for how the hitherto unknown universal functional of the Hohenberg-Kohn theorem can be approached. $F[\rho]$ contains the individual contributions of the kinetic energy, the classical Coulomb interaction and the non-classical portion due to exchange, and electron correlation effects,

$$F[\rho] = T[\rho] + E_H[\rho] + E_{non-classical}[\rho] \tag{3.20}$$

Only $E_H[\rho]$ is known. Kohn and Sham suggested to use expression 3.21 to obtain the exact kinetic energy of the non-interacting reference system with the same density as the real interacting one

$$T_s = -\frac{1}{2} \sum_{i}^{N} < \varphi_i | \nabla^2 | \varphi_i > \tag{3.21}$$

Of course $T_s \neq T$, the true kinetic energy. Then they introduced the following seperation of $F[\rho]$:

$$F[\rho] = T_s[\rho] + E_H[\rho] + E_{XC}[\rho] \tag{3.22}$$

where E_{XC} is so-called *exchange-correlation* energy, rewrite the equation 3.22

$$E_{XC}[\rho] = F[\rho] - T_s[\rho] - E_H[\rho] \tag{3.23}$$

The residual part of the true kinetic energy, which is not covered by T_s, is simply added to the non-classical electrostatic contributions. In other words, the exchange-correlation energy E_{XC} is the functional which contains everything that is unknown. So now we get:

$$\begin{aligned} E[\rho(\vec{r})] &= -\frac{1}{2}\sum_i^N < \varphi_i|\nabla^2|\varphi_i > + \frac{1}{2}\sum_i^N\sum_j^N \int\int |\varphi_i(\vec{r}_i)|^2 \frac{1}{r_{ij}} |\varphi_j(\vec{r}_j)|^2 d\vec{r}_i d\vec{r}_j \\ &+ E_{XC}[\rho(\vec{r})] - \sum_i^N \int \sum_I^M \frac{Z_I}{r_{iI}} |\varphi_i(\vec{r}_i)|^2 d\vec{r}_i \end{aligned} \tag{3.24}$$

Minimize $E[\rho]$ with constant number of electrons, apply the variational principle, result the *Kohn-Sham* equation:

$$\Big(-\frac{1}{2}\nabla^2 + V_{eff}(\vec{r}_i)\Big)\varphi_i = \varepsilon_i \varphi_i \tag{3.25}$$

where

$$V_{eff}(\vec{r}) = [\int \frac{\rho(\vec{r}_2)}{r_{ij}} + V_{XC}(\vec{r}_i) - \sum_I^M \frac{Z_I}{r_{iI}}]\varphi_i \tag{3.26}$$

$$V_{XC} \equiv \frac{\delta E_{XC}}{\delta \rho} \tag{3.27}$$

If the exact forms of E_{XC} and V_{XC} were known (which is unfortunately not the case), the Kohn-Sham strategy would lead to the exact ground state energy. Till now, what we have illustrated in this section does not contain any approximation as of yet. Thus, unlike the Hartree-Fock model, where the approximation is introduced right from the start, the Kohn-Sham approach is in principle exact for the ground state. At this stage, we need to introduce an approximation for the exchange-correlation potential. Assume that ρ is sufficiently slowly varying, one can show that:

$$E_{XC}[\rho] = \int \rho(\vec{r})\epsilon(\rho(\vec{r}))d\vec{r} \tag{3.28}$$

where $\epsilon(\rho)$ is the exchange-correlation energy per electron of a *uniform electron gas* of density ρ, and regard it as known from theories of homogeneous electron gas [28]. Writing E_{XC} in this way defines the *Local Density Approximation*(LDA).

Another alternative of E_{XC} is the *Generalized Gradient Approximation*(GGA). By using not only the information about the density at a particular point, but to supplement the density with information about the gradient of the charge density, $\nabla\rho(r)$ in order to account for the non-homogeneity of the true electron density.

3.1.8 Basis Sets

The preceding sections provided an overview of density functional theory. We now turn to the more practical problem. First of all, we need to chose a basis set for the Kohn-Sham wave functions φ_i. The popular basis sets include plane waves, real space grids, and atomic orbitals etc. The basis set will affect how much memory will be required to store the wave functions and Hamiltonian, and how much run-time will be required to solve for the eigenstates. In addition, the completeness of the basis set will also influence the accuracy of the results.

Plane waves are a natural basis set to use for a periodic system. As is indicated by Bloch's theorem [29], the electronic wave function can be written as:

$$\psi_{ik}(r) = e^{ik\cdot r} \cdot u_i(r) \tag{3.29}$$

where u_i is a periodic function, and k is the Bloch wavevector. Since u_i is a periodic function, we can expand it into a discrete sum of plane waves

$$u_i(r) = \sum_G c_{iG} \cdot e^{iG\cdot r} \tag{3.30}$$

where G are the reciprocal lattice vectors, and c_{iG} are the expansion coefficients. In practice, the sum is terminated at an upper cutoff for G, so that expansion becomes finite but at the same time still accurately represents the wavefunction. Using the above expression for u_i, we can represent the wavefunction as a plane wave sum

$$\psi_{ik}(r) = \sum_G c_{i,k+G} \cdot e^{i(k+G)\cdot r} \tag{3.31}$$

in which c_i are Fourier transform coefficients.

3.1.9 Pseudopotentials

The concept of a pseudopotential [30][31][32] is a crucial one for plane-wave total energy methods since the alternative full Coulomb potential of the electron-ion interaction decays too slowly to be accurately represented by a small number of Fourier components.

The ion cores contain nuclei and tightly bound core electrons. The valence-electron wavefunctions are orthogonal to core-electron wavefunctions. All-electron DFT methods treat core and valence electrons on an equal footing. In the pseudopotential approach ion cores are considered to be *frozen*. This means that properties of molecules or solids are calculated on the assumption that the ion cores are not involved in chemical bonding and do not change as a result of structural modifications.

The pseudopotential approximation replaces core electrons and the strong Coulomb potential by a weaker pseudopotential that acts on a set of pseudo wavefunctions. This potential can be represented with only a small number of Fourier coefficients. Pseudo wavefunctions ideally should have no nodes inside the core regions and thus they only require a small basis set. It is now well known that the combination of the power of plane wave technology and the pseudopotential concept is extremely useful for the description of chemical bonding [33].

3.2 Methods and Computational Details

The DFT calculations were carried out using the CAmbridge Serial Total Energy Package(CASTEP) [34]. Ultrasoft pseudopotentials were employed. Exchange-correlation energy of the valence electrons was treated using both the local density approximation (LDA) and the generalized-gradient approximation (GGA). The wave function was expanded into a plane wave basis set using a cutoff energy of 450 eV. For the integration over the Brillouin Zone, a Monkhorst-Pack $4 \times 4 \times 2$ k-point mesh was used for $g - C_3N_4$, $3 \times 3 \times 2$ for $g - C_6N_8$, $4 \times 4 \times 4$ for $3D - C_3N_4$, and $3 \times 3 \times 3$ for $3D - C_6N_8$, in order to keep the same K-point sampling density. The crystal coordinates by the refinement of the X-ray diffraction data were used as the initial geometries for the geometry optimization. During relaxation, all atomic coordinates were optimized with the constraints of keeping the space group symmetry and freezing the lattice constants.

All calculations were performed at zero K and without time scale. This means that it doesn't include thermochemical corrections such as zero point vibration energy (E_{zpv}) and finite temperature effect. However, since E_{zpv} is much smaller than the internal energy, and the *changes* of zero point vibrational energies between different structures of similar geometry are not significant, the effect of the zero point correction could be neglected.

It should be noted that there are two different exchange correlation functionals(E_{XC}) corresponding to the LDA and GGA treatments. The results by both functionals will be discussed and compared in the following sections. Generally speaking, the results from the LDA calculations will give *c.a.* 1% shorter bond lengths than experimental results. In the other hand, the bond lengths from GGA calculations will be $0-0.5\%$ greater than the experiments. Thus, in most cases GGA has better agreement with the experiments. However, none of these functionals could give reasonable description for the *Van der Waals interaction*: *e.x.* interaction between the graphitic layers. LDA accidentally gives good results for large distance in graphite, GGA almost neglects the *Van der Waals interaction*(close to zero!). Further discussion about this effect will be carried out in the following sections.

3.3 Formation Energy of the Vacancies of Carbon Nitride

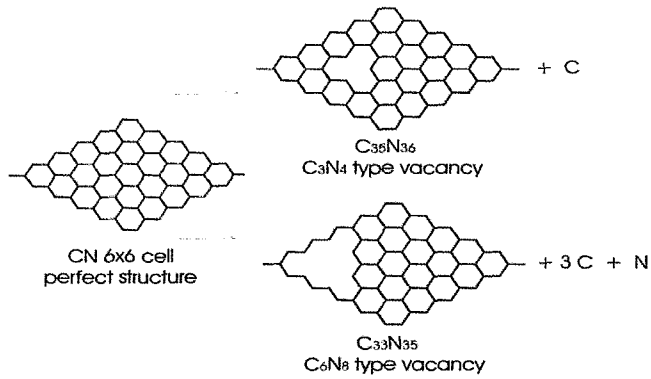

Figure 3.1: Defect structures

Comparing with graphite, the CN 6×6 perfect structure($C_{36}N_{36}$) has

every second carbon exchanged to nitrogen. From the CN 6 × 6 cell, the vacancy of C_3N_4 and C_6N_8 type could be formed (see Fig. 3.1).

The definition of the formation energy E_{form} is:

$$E_{form} = E_{products} - E_{reactant} \tag{3.32}$$

Graphite and nitrogen are taken as reference (reactant). A negative E_{form} means the formation of the material is exothermic and thermochemically favored, and a positive value means the formation of the material is endothermic and thermochemically unfavored. The calculated formation energy (E_{form}) of CN perfect single layer structure is 3037 kJ/mol by LDA, and 5345 kJ/mol by GGA. Both are large positive value, and thus the perfect CN structure is highly unstable with respect to graphite and nitrogen. For

Table 3.2: Formation energy of vacancies

Different structures	E_{form} with E_{XC-LDA} in kJ/mol	E_{form} with E_{XC-GGA} in kJ/mol
C_3N_4 type	- 286	- 537
C_6N_8 type	- 948	- 1185

both C_3N_4 and C_6N_8 types of vacancies, the $E_{form} < 0$ (table 3.2). So the formation of the vacancy in CN is favored and spontaneous.

Figure 3.2 shows C_3N_4 and C_6N_8: the two basic carbon nitride single

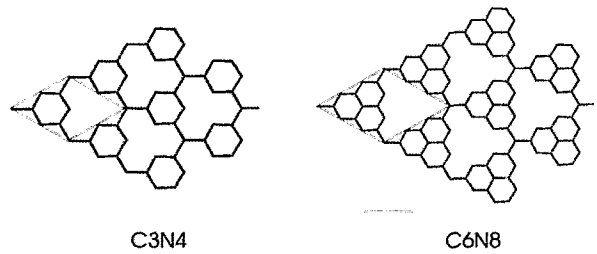

Figure 3.2: Inplane unit cell

layer structures concerned, where green represents carbon atoms and blue represents nitrogen atoms. Here, they have regular vacancies on CN 6 × 6 sheet. The E_{form} of those two types of vacancies are calculated from:

$$CN_{6\times6\ cell} \rightarrow 9\ C_3N_4 + 9\ C \tag{3.33}$$

$$CN_{6\times6\ cell} \rightarrow 4\ C_6N_8 + 12\ C + 4\ C \tag{3.34}$$

The results are listed in table 3.3. Both structures have a large negative

Table 3.3: Formation energy of single layer carbon nitride

Different structures	E_{form} with E_{XC-LDA} in kJ/mol	E_{form} with E_{XC-GGA} in kJ/mol
C_3N_4 type	- 2523	- 3208
C_6N_8 type	-2739	- 3729

value of E_{form}, which means they have tendency to form this kind of vacancy structure from the CN 1:1 stoichiometry structure. Michel and co-workers proposed [19] an explanation for its stability: in order to be a semiconductor, a compound must satisfy the general valence rule:

$$\frac{n_e + b_a - b_c}{n_a} = 8 \tag{3.35}$$

In the above expression n_e is the total number of valence electrons, n_a is the number of anions, b_a is the number of electrons involved in forming anion-anion bonds, and b_c is the number of electrons involved in forming cation-cation bonds (including any "unshared" valence electrons on the cations). All of these values are calculated per formula unit of the compound. This rule expresses the fact that in a semiconducting compound the valence subshell of the s and p electrons(eight) on the anion is filled. It is a generalization of the (8-N) rule which includes more compounds.

In particular for the carbon nitride compounds, it is unfavorable to have N-N bonds since they are so strong they would not contribute to the binding of the structure as a whole and would act as an independent unit. Therefore, we can set $b_a = 0$ in the above formula. For an arbitrary stoichiometry, C_xN_y , we can write $n_a = y$ and $n_e = 4x + 5y$, hence we obtain $b_c = 4x - 3y$. Consider the case of $b_c = 0$ which means that there is no C-C bonds or unshared electrons in the structure. The only stoichiometry satisfies this requirement is C_3N_4. Both C_3N_4 and C_6N_8 have the right stoichiometry to meet this requirement.

3.4 Crystal Structures of Carbon Nitride

3.4.1 Graphitic Carbon Nitride

The graphitic structure $g - C_3N_4$ has been theoretically predicted to be the most stable C_3N_4 form [16][35]. Several other forms of carbon nitride crys-

tal structures could also exist. Recently, another possible building block for C_xN_y has been proposed: tri-s-triazine rings C_6N_7 which are cross-linked by trigonal N atoms [11]. Moreover, as indicated in the previous section, both $g-C_3N_4$ and $g-C_6N_8$have the right stoichiometry, for which the crystal structure will be examined. The inplane unit cell (red rhombus) is shown in Fig 3.2.

The calculated inplane periodicities for the two structures are listed in table 3.4. As mentioned before, LDA gives 0-1% smaller and GGA gives 0-0.5%

Table 3.4: Inplane Periodicity

Structures	with E_{XC-LDA}	with E_{XC-GGA}
$g-C_3N_4$	4.734 Å	4.791 Å
$g-C_6N_8$	7.058 Å	7.130 Å

greater bond length with respect to experiment. Thus, both LDA and GGA calculations give similar results. The differences are less than 0.1 Å. Inplane periodicity of $g-C_3N_4$ is *c.a.* 4.7 Å, and that of $g-C_6N_8$ is *c.a.* 7.1 Å.

Another periodicity in XRD measurement is 6.75 Å (see Fig 2.3), which matches the inplane periodicity for the $g-C_6N_8$ phase. The calculated inplane periodicity for the $g-C_6N_8$ phase is only 0.35 Å greater than the XRD results. For the XRD measurement, the corresponding peak for inplane periodicity is relatively broad. The peak at 6.75 Å is an average value over multiple periodicities. This could explain the slight difference between the GGA calculation results and the XRD data.

As indicated in D.T. Vodak's paper [36], the most stable stacking for $g-C_3N_4$ is an AB stacking, with the second layer rotated by 60° and translated by $\frac{1}{2}$ unit cell (see Fig 3.3). For $g-C_6N_8$, after testing for several different stacking variants, we have found the structure with the lowest energy, as shown in Fig 3.4, with the second layer rotated by 60° and translated by $\frac{1}{3}$ unit cell.

There is no doubt that one of the most important effects in determining the stability of carbon nitrides is the role played by the nonbonded N-N repulsions. These unfavorable electrostatic interactions have already been demonstrated to be relevant in accounting for the stability of some C_xN_y phases. Nitrogen atoms avoid being stacked on top of each other so as to reduce repulsive interactions along the stacking direction, which gives the interaction energy between the layers (E_b) for both structures. In general,

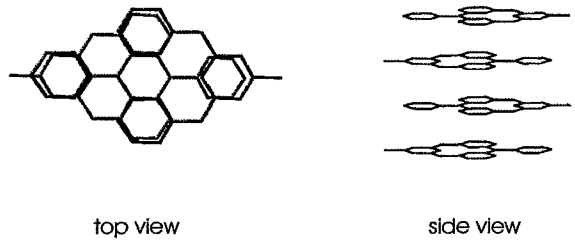

Figure 3.3: $g - C_3N_4$ crystal structure with AB stacking

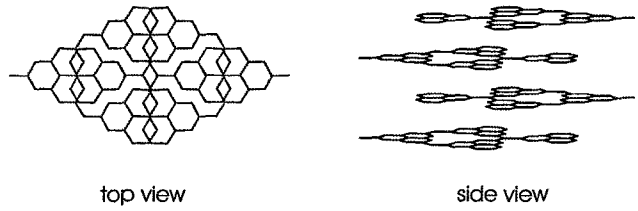

Figure 3.4: $g - C_6N_8$ crystal structure with AB stacking

when DFT comes to *Van der Waals* interaction, LDA accidentaly gives a relatively close value to the experiments. GGA almost neglects all of this weak interaction. So in table 3.5, LDA shows a greater layer-layer interaction and the GGA values are quite small. However, both LDA and GGA give the same trend, that the interaction between the layers of the $g - C_6N_8$ phase is much stronger, almost twice the interaction in the $g - C_3N_4$ phase.

Examining the stacking structure of the two phases carefully, it could be found that for $g - C_3N_4$ phase, three nitrogen atoms are stacking on top of the carbon atoms, and two nitrogen atoms are at the vacancy position. For $g - C_6N_8$, there is no N-C or N-N overlap along the stacking direction, and only three C-C overlap could be observed. Since the nitrogen carries a lone pair of electrons, the C-N repulsion is stronger than C-C. The size of

Table 3.5: Energy of layer-layer interaction

Structures	E_b/atom with E_{XC-LDA}	E_b/atom with E_{XC-GGA}
$g-C_3N_4$	2.69 kJ/mol	0.40 kJ/mol
$g-C_6N_8$	4.69 kJ/mol	1.14 kJ/mol

the nitrogen atom is larger than carbon, which will also increase the C-N repulsion. Thus, both electrostatic and steric hindrances lead to a weaker layer-layer interaction in the $g-C_3N_4$ phase.

The layer distances for the two phases are quite similar (table 3.6), 3.0

Table 3.6: Layer-layer distance

Structures	with E_{XC-LDA}	with E_{XC-GGA}
$g-C_3N_4$	2.997 Å	3.646 Å
$g-C_6N_8$	2.941 Å	3.600 Å

Å for LDA, and 3.6 Å for GGA. Although the two phases have different structure inplane, this difference does not have strong effects on the layer distance. The XRD pattern of carbon nitride (see Fig 2.3) indicates two periodicities, one of which is 3.26 Å. The calculated layer distances for both phases are close to the XRD measurement. Till now, the $g-C_6N_8$ phase fits the experiment results well, at the aspects of both the inplane and interlayer parameters.

3.4.2 Three Dimensional Carbon Nitride

Recently, Vodak and co-workers have examined [36] a new structure of $SrSi_2$ based on the Si network [37]. So far, no literatures have concerned the three dimensional carbon nitride with tri-s-triazine unit. It will be interesting to examine the 3D structure with the building block of C_6N_8.

In the 3D-C_3N_4 structure, the triazine units are linked by three-coordinate nitrogen, in one unit cell, and every next triazine unit is perpendicular to each other(see Fig 3.5 a). In 3D-C_6N_8, however, the three-coordinate nitrogen links three tri-s-triazine units together. The distance between two parallel triazine/tri-s-triazine unit is 4.8 Å for 3D-C_3N_4, and 7.0 Å for 3D-C_6N_8. Again, we get a very familiar distance: 7.0 Å in 3D-C_6N_8 phase.

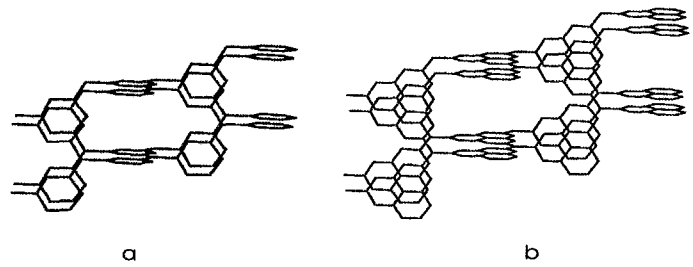

Figure 3.5: Crystal structure of a: 3D-C_3N_4 and b: 3D-C_6N_8

Unfortunately, there is no correspond periodicity to 3.2 Å, the second peak in XRD, observed.

3.5 Cohesive Energy of Carbon Nitride

The next interesting question would be the stability of different phases. Let's look at the Cohesive Energy (E_{coh}) of those structures. E_{coh} is defined as:

$$E_{coh} = -\left(\frac{E_{R0}}{M} - \frac{E_{R\to\infty}}{M}\right) \tag{3.36}$$

E_{coh} is the energy needed in order to dissociate the atoms of a solid (usually a crystal) into isolated atomic species. E_{R0} stands for the energy of the crystal at the equilibrium crystal structure state. $E_{R\to\infty}$ is the energy of isolated atoms after dissociation. M is the number of atoms. E_{coh} is an important parameter shows which crystal structure the solid will adopt, namely the one with the highest E_{coh}(which is nothing but the system achieving the lowest total energy). In general, the LDA calculation gives a much higher E_{coh} than GGA.

Before we start, let's compare the E_{coh} of $g - C_3N_4$, the most investigated

Table 3.7: E_{coh} from different work

	Ref. [14]	Ref. [18]	This work
E_{coh} of g-C_3N_4 per atom kJ/mol	659.6	683.3	667.4

phase of carbon nitride, between our calculations and literature reported values. This could be used to examine the quality of our calculation results. All

data in table 3.7 were calculated with E_{EX-LDA}. E_{coh} of $g-C_3N_4$ from our calculation is between those two literature values, which suggests that our calculation result is reasonable.

The calculated cohesive energies for graphite and different phases of carbon

Table 3.8: Cohesive energy of C_xN_y Phases

Structures	E_{coh}/atom with E_{XC-LDA} kJ/mol	E_{coh}/atom with E_{XC-GGA} kJ/mol
$g-C_3N_4$	667.4	570.6
$g-C_6N_8$	672.1	576.4
3D-C_3N_4	672.8	579.6
3D-C_6N_8	674.3	582.7
graphite	852.5	754.0

nitride are given in Table 3.8. E_{coh} of all the carbon nitrides are much smaller than graphite, and thus are much less stable.

For *graphitic* carbon nitride, both LDA and GGA calculations suggest that the E_{coh} for $g-C_6N_8$ is greater than $g-C_3N_4$, so it is more stable. The difference of E_{coh} between the two phases is *c.a.* 5-6 kJ/mol per atom. The different stabilities of the two phases may be due to the difference in the interlayer interaction or inplane bonding energy.

The discussion above (table 3.5) suggests that the interlayer repulsion energy in $g-C_6N_8$ is smaller than that in $g-C_3N_4$. The difference is *c.a.* 1-2 kJ/mol per atom. This is a minor contribution to the greater stability of $g-C_6N_8$. The difference of inplane bonding energies is the major contribution to the stability. The aromatic system of *tri-s-triazine* unit is larger than that of *triazine*. The electrons are delocalized in a larger system. The stronger homo-conjugation leads to a lower inplane bonding energy.

For the *three dimensional* case, in both LDA and GGA calculations, the differences between 3D-C_3N_4 and 3D-C_6N_8 are similar (table 3.8), which is about 2-3 kJ/mol per atom. The C_6N_8 phase is more stable than the C_3N_4 phase. In the C_6N_8 phase, the N $\cdots$ N distance for every two parallel tri-s-triazine unit is 7.0 Å, whereas such a distance in the C_3N_4 phase is 4.8 Å. The far separation of N $\cdots$ N stabilizes the lone pair electrons repulsion of nitrogen. In the other hand, the large aromatic system delocalizes the electrons inplane. Thus, among the 3D structures, the C_6N_8 phase is more

stable, too.

The higher the E_{coh}, the more stable the structure is. It is clear that 3D-C_6N_8 is the most stable one among the four phases both in LDA and GGA. LDA value are higher than GGA calculation, it is a normal situation. But still, the energy difference between every phases are quite small, which is between 1-5 kJ/mol per atom.

3.6 Comparison

For easier comparisons, we take the structure with the lowest E_{coh}, 3D-C_6N_8, as reference point, to plot the difference of E_{coh} as a function of density (see Fig 3.6). The density is calculated from:

$$\rho = \frac{number\ of\ atoms\ in\ unit\ cell}{volume\ of\ unit\ cell} \tag{3.37}$$

Both LDA and GGA give the same trend. While density decreasing, the

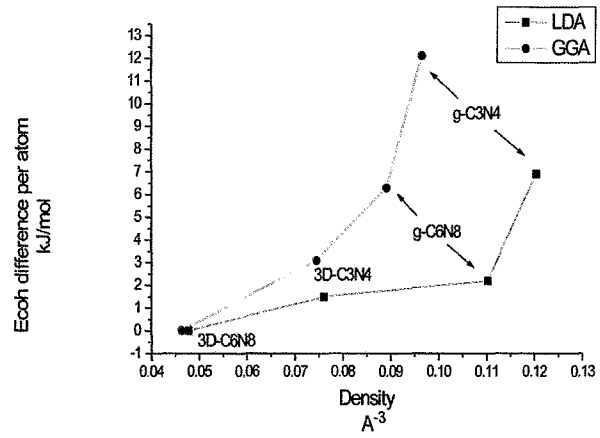

Figure 3.6: Relatives stability of CNx models

stability increases. The density of graphite is 0.11 $Å^{-3}$ in LDA, and 0.08 $Å^{-3}$ in GGA. It is between the density of 3D-C_3N_4 and $g - C_6N_8$. In general, the 3D phases are more stable than the graphitic phase. In 3D-C_3N_4, each triazine unit has one N$\cdots$N repulsion, whereas three such interactions are

introduced by the fully planar arrangement present in the $g - C_3N_4$ phase. It is the same for the two C_6N_8 phases. This indicates that the graphitic structures are experiencing destabilizing strain due to several close N$\cdots$N nonbonding distances.

Due to the small energy differences of each phase, we can make the only conclusion that 3D-C_6N_8 is the most favored structure, but the other phases may also exist. All the discussion above was based on the thermochemical theory. It is possible that the most stable product could not be formed due to high activation energy. Thus, kinetics calculations need to be carried out to study the properties of the transition state structures, reaction rates, and to gain further understanding about the polymerization mechanisms.

3.7 Thermodynamic Stability: Polymerization Mechanism

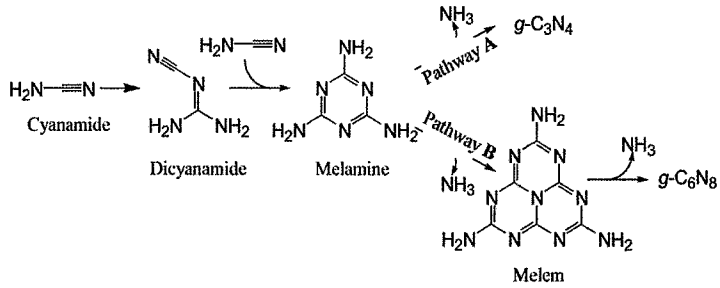

Figure 3.7: Polymerization pathways for both CNx models

Considering the possibility to synthesize carbon nitrides, one also has to account for their thermochemical stability with respect to the starting materials. Density functional calculations have been carried out to study the phase stability for the CNx models. However, since our goal is to provide only a general thermochemical tendency for the two stoichiometries, we have decided to discuss our investigation only with the GGA calculations. The reaction enthalpies for both model systems have been studied (Fig 3.7).

The polymerization energy profiles for both reactions are given in Figure 3.8. The relative enthalpies of formation at 0K (ΔH_f, in kJ/mol) are with

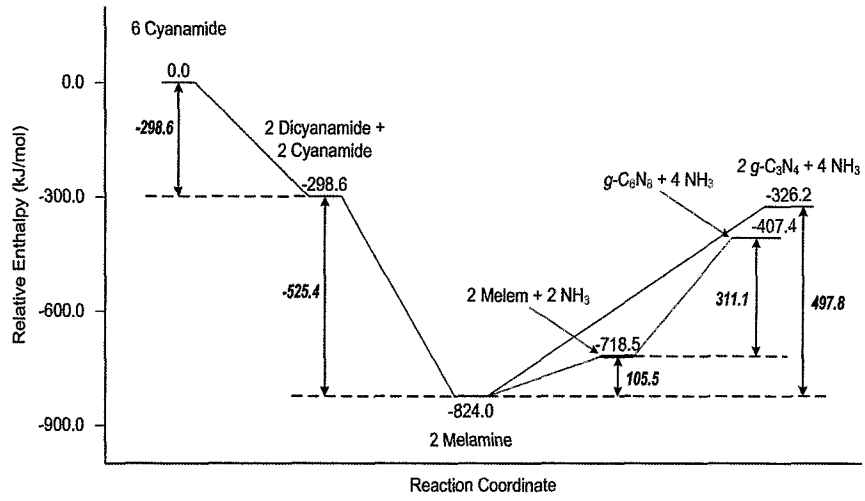

Figure 3.8: Polymerization energy profiles for the reactions for the CNx model systems

respect to the reactant, 6 moles cyanamide. The reaction enthalpies for each step are given in italic. Both pathways start from 6 moles cyanamide. The product of pathway A is 2 moles $g - C_3N_4$ and 4 moles NH_3. The product of pathway B is 1 mole $g - C_6N_8$ and 4 moles NH_3.

Pathway A and pathway B follow the same procedures for the first two steps, the dimerization of cyanamide and the formation of melamine. Both steps are exothermic. The reaction enthalpies are -298.6 kJ/mol and -525.4 kJ/mol, respectively. The third step for pathway A, the formation of $g - C_3N_4$ from melamine, is endothermic. The reaction enthalpy is 497.8 kJ/mol. The third and forth steps for pathway B, the formation of melem and the formation of $g - C_6N_8$, are also endothermic. The reaction enthalpies are 105.5 kJ/mol and 311.1 kJ/mol, respectively. The energy needed for the third step for pathway A (497.8 kJ/mol) is much higher than that for pathway B (105.5 kJ/mol). This suggests that pathway B is thermochemically favored over pathway A at this step. The products for both pathways are more stable than the reactants. The relative energies for the products with respect to the reactants are -326.2 kJ/mol for pathway A, and -407.4 kJ/mol for pathway B. The product for pathway B, $g - C_6N_8$, are 81.2 kJ/mol more stable than the product for pathway A, 2 moles $g - C_3N_4$. This suggests that pathway B is thermochemically favored over pathway A, and $g - C_6N_8$ is the major product for the polymerizations.

The calculation results are in a qualitative agreement with the DSC measurement (Figure 2.1). The first two steps are exothermic, and the last two steps are endothermic.

Chapter 4

Summary and Outlooks

This thesis presents an experimental and theoretical study of the structural and electronic properties of carbon nitrides. The carbon nitride was synthesized by polymerization of various monomers including cyanamide and pyrazine carbonitrile. The crystal structure was revealed by the XRD and HRTEM analysis. Both results show two periodicities: 6.75 Å and 3.26 Å. The periodicity at 6.75 Å has hexagon periodicity feature, and 3.26 Å is close to the layer distance of graphite (d = 3.35 Å). Thus, it could be predicted from these experimental results that the product is graphitic carbon nitride with a 6.75 Å inplane periodicity and a 3.26 Å layer distance.

The experimental work was complemented by DFT calculations to determine the most stable structure of carbon nitride. Four different structures of carbon nitride were investigated in order to give the relative stability. $3D - C_6N_8$ has the lowest cohesive energy among the four phases, and thus it is the most stable form. However, the difference of the cohesive energies between different phases are relatively small, so the other phases may also exist in the crystal structure. According to the calculated crystal parameters of these four structures, g-C_6N_8 has a 7.1 Å inplane hexagon periodicity, and a 3.0 Å layer distance, which gives the best agreement with XRD and HRTEM data. This indicates that the major product of the synthesis may be graphitic carbon nitride g-C_6N_8, even though the $3D - C_6N_8$ has a lower energy. It should be mentioned that no vibrational contributions or entropic effect were considered in the calculations and there might be kinetic effects during the growth which might trap the material in a metastable state.

Using cyanamide as monomer, the polymerization mechanism has been rationalized by DSC and XRD. In the mean time, DFT calculations were carried out to study the thermal condensation mechanism. It has a quantitatively

agreement with the DSC measurement. For the polymerizations to form $g-C_6N_8$ and $g-C_3N_4$, the first two exothermic steps from cyanamide to melamine are the same. Then the melamine intermediate favors to form the $g-C_6N_8$ phase which has a lower internal energy than the previously suggested $g-C_3N_4$. For the polymerization starting from pyrazine, pyrazine carbonitrile was introduced as a new monomer for carbon nitride materials. TEM result suggests that heat treatment of this monomer yields two different crystalline species. Temperature dependent XRD experiments showed the transformation of liquid PCN at room temperature to a well defined organic crystal at 350°C. By increasing the temperature up to 550°C, a graphite analogous structure was formed.

After thoroughly studying the synthesis pathways and crystal structures for carbon nitride, the applications of CN as catalyst support were also investigated experimentally. Different pathways were followed by mixing monomers, intermediate structures, or the ready-made g-C_xN_y with metal salts. Heat treatment of these materials with the metal salts yields in a partial destruction of the structures, due to oxidation of the organic material. Mixing bulk g-C_xN_y with metal salts in solution, partially incorporated metal ions could be formed. As one crucial parameter, for the amount of included salt, the reaction temperature was identified. Photoluminescence and excitation spectra indicate a strong interaction of the cyamellur cores with the metal ions, which could be explained by a complexation of the metal ions in the voids of the C_xN_y layers.

We get a very interesting result from the calculated heat of formation of carbon nitride. The heat of formation for these four structures are all greater than zero. That means these phases are all metastable, and have the tendency to dissociate and form graphite and nitrogen gas. This metastability, although may decrease the stability of the material, suggests that these materials are possible to eliminate nitrogen and form a phase consists of pure carbon, which could be expect as a new morphology of nanoporous carbon. The use of this nanoporous carbon materials may provide new opportunities for catalyst development, etc. Of course, there is still a lot of work to be done to gain the comprehensive understanding of carbon nitride materials.

Acknowledgments

First of all, I would like to thank both of my supervisors: Professor Markus Antonietti for recruiting me and allowing me to take part in his groundbreaking research, and Professor Matthias Scheffler for showing me the beauty and power of theoretical world.

I am indebted to Dr. Johan Carlsson for his supervision, and training with computational and DFT method , from the basic theories to their applications, and also for his carefully examining this thesis. I also want to express my gratitude to Dr. Arne Thomas, not only for the supervision in experimental work but also his ability to find meaningful interpretations behind the experimental results. Without their help, none of this work could be done.

I am grateful for all of other group members, especially Christoph Freysoldt who has always been helping me with the coding problems and answering my questions about using Latex, Serdar Durdagi who has been helping me use the CASTEP code, and Xinzheng Li who gave me his encouragement when I was frustrated.

At Last, a special thanks to my parents, who have always been behind me and supported me over the years.

Bibliography

[1] E. Kroke, M. Schwarz. *Coordination Chemistry Reviews.* 248 (2004) 493-532

[2] B.L. Ivanov, L.M. Zambov, G.T. Georgiev, C. Popov, M.F. Plass, W. Kulisch, *Chem. Vap. Deposit.* 5 (1999) 265.

[3] S. Xu, S. Kumar, Y.A. Li, N. Jiang, S. Lee, *J. Phys.: Condens. Matter.* 12 (2000) L121.

[4] M. Aono, S. Nitta, T. Iwasaki, H. Yokoi, T. Itoh, S. Nonomura, *Mater Res. Soc. Symp. Proc.: Low-Dielectr. Const. Mater.* V 565 (1999) 291.

[5] Z. Zhang, H. Guo, Y. Xu, W. Zhang, X. Fan, J. *Mater. Sci. Lett.* 18 (1999) 685.

[6] J. Wei, P. Hing, Z.Q. Mo, *Wear.* 225-229 (1999) 1141.

[7] M. Akiyama, I. Alexandrou, M. Chhowalla, G.A.J. Amaratunga. *J.Mater. Sci.* 36 (2001) 5397.

[8] J. Kouvetakis, A. Bandari, M. Todd, B. Wilkens, N. Cave. *Chem. Mater.* 6 (1994) 811.

[9] Q. Lu, C. Cao, C. Li, J. Zhang, H. Zhu, X. Kong, X. Duang. *J. Mater. Chem.* 13 (2003) 1241.

[10] Z. Zhang, K. Leinenweber, M. Bauer, L.A.J. Garvie, P.F. McMilla, G.H. Wolf. *J. Am. Chem. Soc.* 123 (2001) 7788.

[11] T. Komatsu, T. Nakamura. *J. Mater. Chem.* 11 (2001) 474.

[12] E. Kroke, M. Schwarz, P. Kroll, E. Bordon, B. Noll, A. Norman. *New J. Chem.* 26 (2002) 508.

[13] Y. Guo, W.A. Goddard III. *Chem. Phys. Lett.* 237 (1995) 72.

[14] A.Y. Liu, M.L. Cohen. *Science.* 245 (1989) 841.

[15] P. Kroll, R. Hoffmann. *J. Am. Chem. Soc.* 121 (1999) 4698.

[16] D.M. Teter, R.J. Hemley. *Science.* 271 (1996) 53.

[17] D.T. Vodak, K. Kim, L. Iordanidis, P.G. Rasmussen, A.J. Matzger, O.M. Yaghi. *Chem. Eur. J.* 9 (2003) 4197.

[18] M. Mattesini, S. F. Matar, *Phys. Rev. B.* 65, (2001) 075110.

[19] M. Cote, M.L. Cohen, *Phys. Rev. B.* 55, (1997) 5684-5688.

[20] Jurgens. B., Irran. E., Senker. J., Kroll. P., Muller. H., Schnick. W. *J. Am. Chem. Soc.* 2003 125(34) 10288-10300.

[21] M. Groenewolt, M. Antonietti, *Advanced Materials.* submitted

[22] W. Koch, M.C. Holthausen *A Chemist's Guide to Density Functional Theory,*Wiley-VCH, ISBN 3-527-30372-3

[23] L. H. Thomas, *Proc. Camp .Philos. Soc.* 23, (1927) 542-548.

[24] E. Fermi, *Rend Accad. Naz. Lincei.* 6, (1927) 602-607.

[25] P. Hohenberg, W. Kohn, *Phys. Rev.* 136, (1964) B864-B871.

[26] H. Eschrig, *The Fundamentals of Density Functional Theory.* (1996)

[27] W.Kohn, L.J. Sham, *Phys. Rev.* 140, (1965) A1133-A1138.

[28] D.Pines, *Elementary Excitations in Solids.* W.A. Benjamin, Inc. 1963

[29] Charles Kittel, *Introduction to Solid State Physics.* 2005

[30] D. Vanderbilt, *Phys. Rev. B.* 41, (1990) 7892-7895.

[31] K. Lassonen, R. Car, C. Lee, D. Vanderbilt, *Phys. Rev. B.* 43, (1991) 6796-6799.

[32] K. Lassonen, A. Pasquarello, R. Car, C. Lee, D. Vanderbilt, *Phys. Rev. B.* 47, (1993) 10142-10153.

[33] G.P. Srivastava, D. Weaire, *Adv. Phys.* 26 (1987) 463-517.

[34] M.D. Segall, P. Lindan, M.J. Probert, *J. Phys.: Condens. Matter.* 14, (2002) 2717-2744.

[35] M. Mattesini, S. F. Matar, A. Snis, J. Etourneau, and A. G. Mavromaras, *J. Mater. Chem.* 9, (1999) 3151.

[36] D.T. Vodak, K. Kim, L.Iordanidis, P.G. Rasmussen, A.J. Matzger, O.M. Yaghi, *Chem. Eur. J.* 9,(2003) 4197-4201.

[37] M. O'Keeffe, M. Eddaoudi, Hailian Li, T. Reineke, O. M. Yaghi, *J. Solid State Chem.* 152, (2000) 3-20.